

## Triple Emission of 5'-(*para*-R-Phenylene)vinylene-2-(2'-Hydroxyphenyl)benzoxazole (PVHBO) – Part II – Emission from the Anions

Joseph J. M. Hurley,<sup>†</sup> Quinton J. Meisner,<sup>†</sup> Peijun Guo,<sup>‡</sup> Richard D. Schaller,<sup>‡</sup> David J. Gosztola,<sup>‡</sup> Gary P. Wiederrecht,<sup>‡</sup> and Lei Zhu<sup>†</sup>

<sup>†</sup> Department of Chemistry and Biochemistry, Florida State University, 95 Chieftan Way, Tallahassee, FL 32306-4390, United States

<sup>‡</sup> Center for Nanoscale Materials, Argonne National Laboratory, Lemont, IL 60439, United States

[lzhu@fsu.edu](mailto:lzhu@fsu.edu)

**Abstract.** This paper is the second part of a study on the effects of substituted 5'-phenylenevinylene (PV) functionality on the emission properties of 2-(2'-hydroxyphenyl)benzoxazole (HBO) – a dye that is known for excited state intramolecular proton transfer (ESIPT). The topical compounds are referred to as **PVHBOs**, each of which is a structural fusion of the HBO component and a 4-hydroxy-4'-R-stilbene fluorophore that meet at the hydroxyphenyl moiety. Therefore, the resulting fusion fluorophore is expected to manifest the properties of one component or the other as governed by its interactions with the environment. In Part I (the preceding paper), **PVHBOs** are divided into two groups depending on whether the R substituent is electron-donating/neutral (Group I) or electron-withdrawing (Group II). The difference in absorption and emission properties between Groups I and II are explained based on observations from spectroscopic experiments (both steady state and time-resolved) and quantum chemical calculations. In the current paper, the same set of tools are applied to characterize the photophysical properties of the conjugate bases – i.e., the anions – of **PVHBOs**. The emission energy of the anion of any Group I compound, where the R group is either electron-donating or neutral, is situated between those of the neutral enol and keto forms. The emission of the anion of any given Group II compound, on the other hand, has a lower energy than both the enol and keto emissions. The frontier molecular orbitals (i.e., HOMO, LUMO, LUMO+1) of a **PVHBO** that localize on either the HBO or the stilbenoid are impacted by the R substituent and solvent/additive differently, which leads to the differences in the optical properties of Groups I and II **PVHBOs** in both neutral and anion forms.

## Introduction

Fluorophores that tend to undergo excited state intramolecular proton transfer (ESIPT) offer two emission bands – one from the unaltered molecular structure (the normal emission), while the other from the proton-transferred excited state tautomer (the tautomer emission).<sup>1-5</sup> The emissions of the normal and the tautomer forms can be tuned to blue and green primary color regions of the visible spectrum, respectively, when an ESIPT core is properly substituted. One type of such compounds was reported in the Part I of this work (the preceding paper),<sup>6</sup> which are the ESIPT-capable compound (2'-hydroxyphenyl)benzoxazoles (HBOs)<sup>7,8</sup> substituted at 5'-position with *para*-R-phenylenevinylene (**PVHBOs**, Figure 1). **PVHBOs** are considered as fusions of the HBO component and a R-substituted stilbenoid dye. A purpose of the current work is to study how the R group influences the emission of the conjugate base of a **PVHBO**, and whether the last primary color, red, could be generated by deprotonation of a **PVHBO**. If that could be done, three primary colors – blue, green, and red – may be materialized using a single fluorophore. Beyond the specific description of the properties of **PVHBOs**, this work demonstrates the involvement of acid/base chemistry in the ground state as another option to control the emission color of an ESIPT dual-emitting dye. As described in Part I, developing multiple emission fluorophores is fundamentally challenging and interesting, while products with new and potentially useful properties might be further modified to meet industrial benchmarks as components of organic light-emitting diodes.<sup>9-11</sup> The challenges on the fundamental front and the likelihood of new utilities of the finished products have provided motivations for completing this work.

In Part I,<sup>6</sup> we reasoned that in order to develop a dye that emits in three primary colors, a lead fluorophore that is capable of producing three emission bands ought to be identified, based on which structural modifications could be carried out to tune the three bands to primary colors. The lead compound that we selected was HBO, while the structural modification that we elected to execute was the installation of a R-substituted phenylenevinylene (PV) group at the 5'-position (Figure 1). In a solvent not competitive in hydrogen bonding, HBO maintains an intramolecular hydrogen bond (HB), by which the ESIPT occurs to afford the tautomerized dye that emits around 475 nm (i.e., the keto emission). The emission of the normal structure centering at ~ 370 nm (i.e., the enol emission) becomes the major component in a hydrogen bonding-capable solvent, because within the solvent/HBO complex the linchpin for ESIPT which is the intramolecular HB is no longer present. When the unsubstituted HBO is deprotonated, the emission of the anion is found at 450 nm. Therefore, HBO is able to provide three emission bands that cover from near-UV (the enol emission) to cyan color (the keto emission). In Part I

(the preceding paper),<sup>6</sup> the enol and keto emissions of the PV-modified HBO molecules (**PVHBOs**) appear in the blue and green regions. In Part II, structural factors that would provide a red-emitting anion are determined.

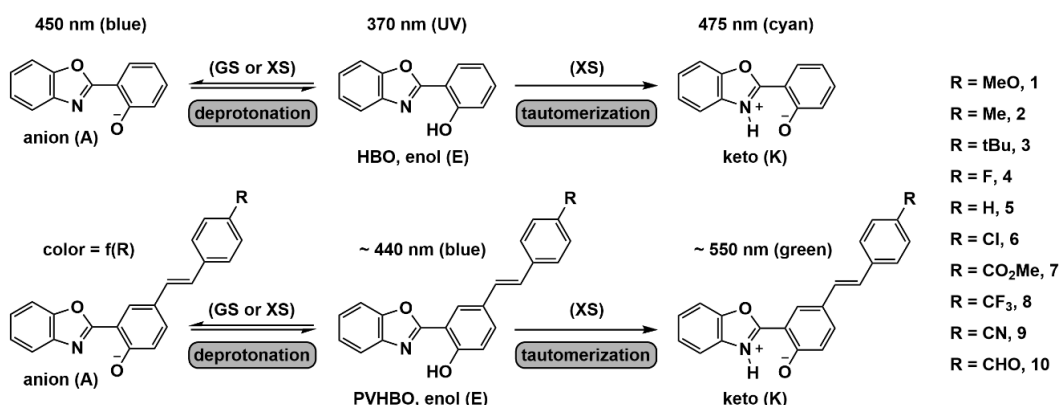


**Figure 1.** Three emission bands of HBO and 5'-(4-R-phenylenevinylene)HBO (**PVHBO**): enol (E), keto (K), and anion (A). GS = ground state  $S_0$ ; XS = first excited state  $S_1$ . The compounds are numbered in the order of increasing  $\sigma_p^+$  values of R groups.

## Results

**Molecular design.** Fusing HBO and a substituted stilbenoid at the hydroxyphenyl moiety creates the **PVHBO** compounds listed in Figure 1. The difference among these compounds is the electronic nature of the R-substituent. As shown in Part I,<sup>6</sup> the neutral **PVHBOs** are capable of solvent-modulated ESIPT similar to HBO – namely, two emission bands of a **PVHBO** were observed in a solvent-dependent manner. The keto emission originates from the intramolecularly hydrogen bonded ground state, while the enol emission results from the excitation of the solvated **PVHBO** without an intramolecular HB. Unlike HBO, upon deprotonation of a **PVHBO**, these compounds may act similarly to phenolate-containing stilbene fluorophores, a consequence of which would be the appearance of a charge transfer-type emission from the anion when the R group becomes increasingly e-withdrawing.

**Absorption of the anions.** Compounds **1-10** were deprotonated using the organic base 1,8-diazabicyclo[5.4.0]undec-7-ene (DBU) in DMSO. As an example, the progressive changes of the

absorption spectrum upon the addition of DBU up to 30 molar equivalents in a sample of **5** (R = H) are shown in Figure 2. The evolution of the absorption spectrum of **5** during a similar DBU titration experiment in acetonitrile is shown in Figure S1. The absorption band at 312 nm decreases as the band at 389 nm increases, correlating with a production of the phenolate at the expense of the neutral phenol form. The shift of absorption to a longer wavelength was expected,<sup>12,13</sup> and was replicated in the rest of the **PVHBOs**. As shown in Figure 3, the anions of the derivatives with more e-withdrawing R-groups (**7**, **9**, and **10**; i.e., the Group II compounds as defined in Part I<sup>6</sup>) have significantly longer absorption wavelengths, consistent with stronger charge transfer-type absorption transitions.

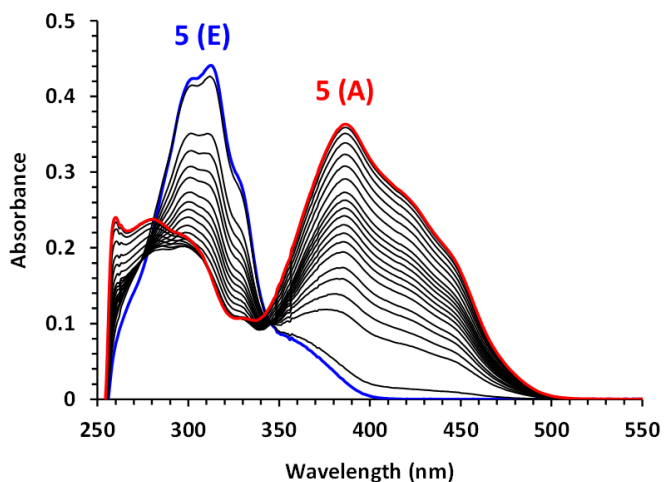


**Figure 2.** Absorption response of **5** (R = H, 10  $\mu$ M) in DMSO titrated with DBU up to 30 molar equivalents. E: the neutral enol form; A: anion. [DBU] = 0-300  $\mu$ M (blue to red).

In addition to the red-shift of absorption maxima of **PVHBO** anions as the R group becomes more e-withdrawing, the profile of the absorption band also undergoes conspicuous changes (Figure 3). Each of the Group I compounds **1-5** features a major absorption band with a shoulder on the long wavelength side, while Group II compounds **7**, **9**, and **10** have the opposite profiles where the shoulder is on the short wavelength side of the main band. The absorption profiles of the deprotonated compounds **6** and **8** appear to be the transitioning cases between Groups I and II.

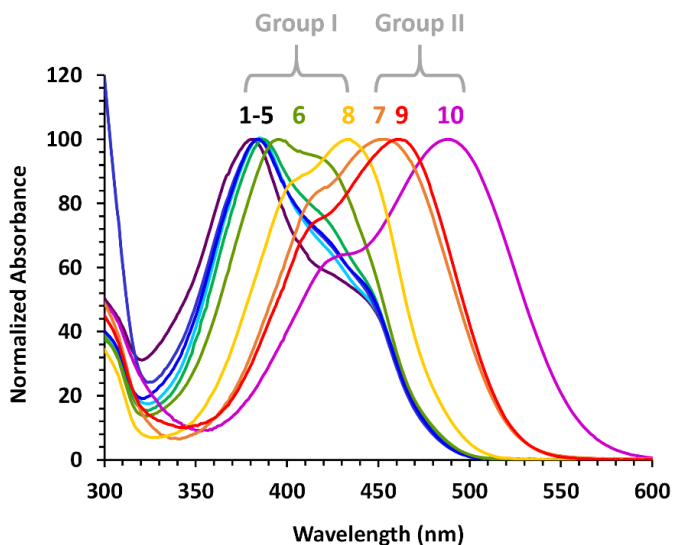


**Figure 3.** Normalized absorption spectra of the anions of **1-10** in DMSO, **1** (R = OMe, violet), **2** (R = Me, navy), **3** (R = tBu, cyan), **4** (R = F, blue), **5** (R = H, green), **6** (R = Cl, yellow-green), **7** (R = CO<sub>2</sub>Me, orange), **8** (R = CF<sub>3</sub>, yellow), **9** (R = CN, red), **10** (R = CHO, magenta); [dye] = 10  $\mu$ M, [DBU] = 30 molar equivalents. The expansion in the Group I region is shown as Figure S2.

**Emission of the anion.** The emission spectra of **5** (R = H) in DMSO over the course of the DBU titration are shown in Figure 4a. The 421-nm-centered band from the neutral enol form, which was dominant in DMSO in the form of a DMSO-hydrogen bonded complex,<sup>6</sup> decreased while a new emission band centering at 504 nm grew as DBU was added. To distinguish the emission of the anion from the keto emission (543 nm) arising from the ESIPT process, the same titration was carried out in acetonitrile (Figure 4b), which showed the decline of the keto band and a similar increase of an emission band at 504 nm. The excitation wavelengths of both titration experiments were selected at the isosbestic points in the absorption mode. Therefore, the increased intensity of emission upon the addition of DBU suggests that the fluorescence quantum yield of the anion is higher than that of the neutral form in both solvents. The normalized emission spectra of the anions of **1** to **10** are shown in Figure 5. The spectra of anions **1-6** tightly overlap and maximize at  $\sim$  500 nm, while those of **7-10** are progressively shifted to longer wavelengths. The anions exhibit sharply different behaviors between the previously defined Groups I (**1-6** and **8**) and II (**7**, **9**, and **10**).

The Group II anions have emission wavelength maxima well past 500 nm, while the emission peaks of the Group I anions are clustered around 500 nm. These results are recorded in Table 1. The excitation spectra are similar to the absorption spectra (Figure S3). Anions of Group II have the longest emission wavelengths with values of 568, 577, and 641 nm for R = CO<sub>2</sub>CH<sub>3</sub> (**7**), CN (**9**), and CHO (**10**), respectively. The fluorescence quantum yields of Group I anions were found within 0.2-0.3 in DMSO, while those of Group II anions (**7**, **9**, **10**) are higher within 0.3-0.5 (Table 1). These values are significantly larger than those of the neutral forms in DMSO, which are at best measured at 0.11.

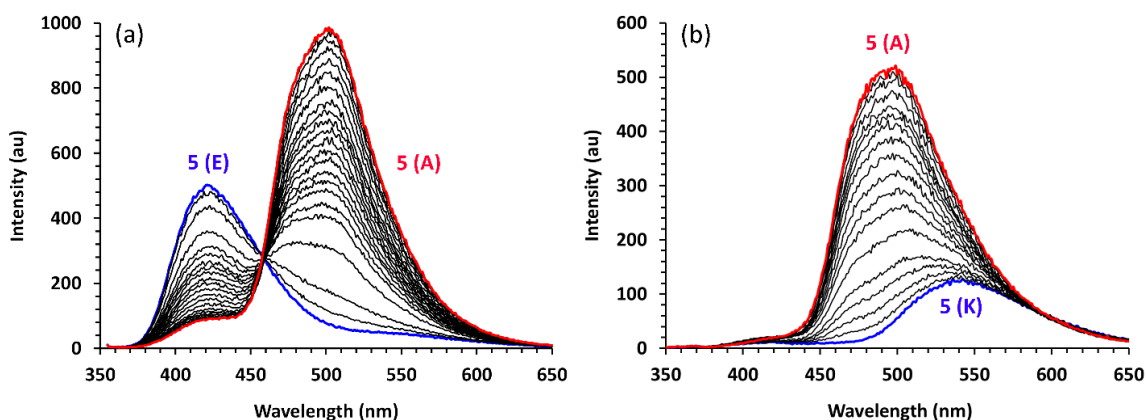


**Figure 4.** (a) Fluorescence response of **5** (R = H, 10  $\mu$ M) in (a) DMSO titrated with DBU up to 30 molar equivalents. E: enol; A: anion; K: keto.  $\lambda_{\text{ex}}$  = 345 nm, [DBU] = 0-300  $\mu$ M (blue to red); and in (b) ACN with DBU up to 100 molar equivalents.  $\lambda_{\text{ex}}$  = 332 nm, [DBU] = 0-1,000  $\mu$ M (blue to red).

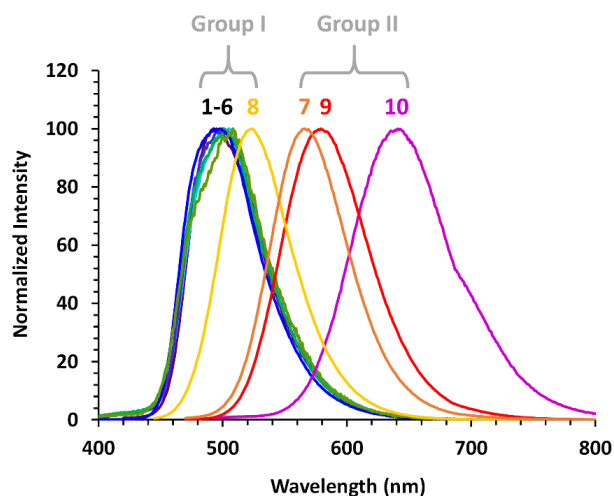


**Figure 5.** Normalized fluorescence emission spectra of the anions of **1-10** in DMSO, **1** (R = OMe, violet), **2** (R = Me, navy), **3** (R = tBu, cyan), **4** (R = F, blue), **5** (R = H, green), **6** (R = Cl, yellow-green), **7** (R = CO<sub>2</sub>Me, orange), **8** (R = CF<sub>3</sub>, yellow), **9** (R = CN, red), **10** (R = CHO, magenta); [dye] = 10 μM, [DBU] = 30 molar equivalents,  $\lambda_{\text{ex}}$  is varied. The spectra of **1-6** closely resemble one another, which makes it difficult to distinguish in this Figure.

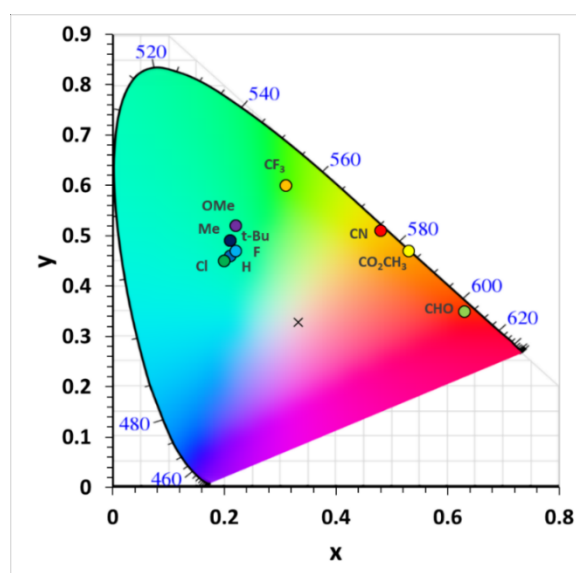


**Figure 6.** CIE 1931 color space diagram of the anions of **1-10** in DMSO. The identities of the R substituents are marked on the graph. White-light reference point: (x,y) = (0.33, 0.33) (x), [dye] = 0.5 μM, [DBU] = 15 μM,  $\lambda_{\text{ex}}$  = 370 nm (Group I), 450 nm (Group II).

**Table 1.** Spectroscopic properties of the anions of **1-10** in DMSO. Group II compounds are shaded.

| Comp. # | R Group                         | $\sigma_p^+$ | $\lambda_{\text{abs}}$ (nm) <sup>a</sup> | $\lambda_{\text{em}}$ (nm) | $\Phi^b$ |
|---------|---------------------------------|--------------|--|----------------------------|----------|
| 1       | OMe                             | -0.78        | 382                                      | 495                        | 0.33     |
| 2       | Me                              | -0.31        | 386                                      | 500                        | 0.31     |
| 3       | t-Bu                            | -0.26        | 386                                      | 503                        | 0.29     |
| 4       | F                               | -0.07        | 385                                      | 498                        | 0.27     |
| 5       | H                               | 0            | 389                                      | 504                        | 0.30     |
| 6       | Cl                              | 0.11         | 396                                      | 508                        | 0.22     |
| 7       | CO <sub>2</sub> CH <sub>3</sub> | 0.49         | 454                                      | 577                        | 0.52     |
| 8       | CF <sub>3</sub>                 | 0.61         | 434                                      | 523                        | 0.20     |
| 9       | CN                              | 0.66         | 463                                      | 568                        | 0.33     |
| 10      | CHO                             | 0.73         | 490                                      | 641                        | 0.35     |

a. Wavelength of maximal intensity beyond 320 nm; b. absolute emission quantum yield.

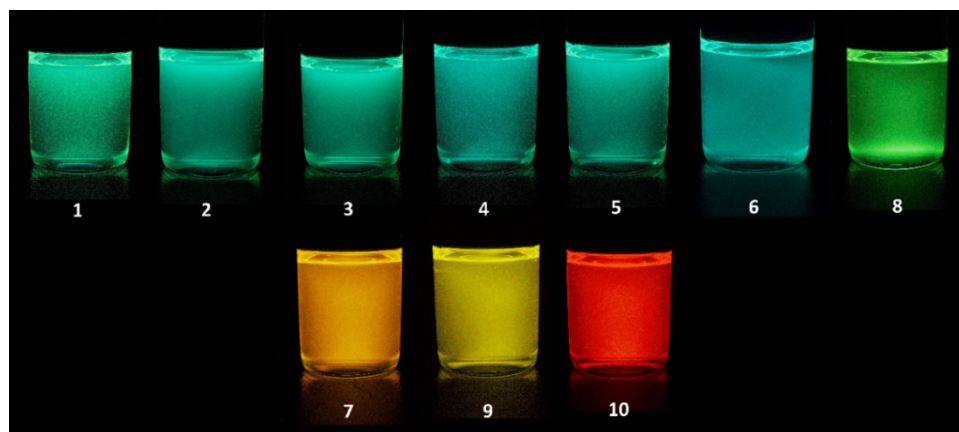


**Figure 7.** Photographs of the **PVHBO** anions in DMSO irradiated using a handheld UV lamp ( $\lambda_{\text{ex}} = 365$  nm). Top: Group I; bottom: Group II. [dye]  $\sim 60$   $\mu\text{M}$ .

**Emission colors and CIE diagrams.** The emission color profiles of the anions of **PVHBOs** in DMSO were mapped on the CIE 1931 XYZ color space (Figure 6). Anions **1-6** have CIE 1931 coordinates that cluster in the cyan-teal region, while anions of **7-10** follow the curved edge on the outside of the coordinate space (i.e., the gamut), indicating that the anions are relatively monochromatic in their emission profile and narrow in their emission bandwidths. The photographs (Figure 7) of the emission of the anions show the difference between members of Groups I and II: all Group I anions (top row) emit in green, while Group II anions (bottom row) emit at longer wavelength regions up to red (i.e., anion of **10**).

**Ultrafast time-resolved emission and absorption spectroscopies.** The time-resolved emission (TE) and absorption (TA) experiments were done on samples of **PVHBOs** in DMSO in the presence of the organic base DBU (20 molar equivalents). The TE data were collected using a Hamamatsu C5680 streak camera that characterizes the “short” and “long” decays within different time windows. The short time window offers a time resolution at  $\sim 2$  ps, while within the long time window photons are captured with a time delay of up to 2 ns. The TA data were acquired on an Ultrafast Systems TA spectrometer (Helios) with a  $\sim 100$ -fs temporal resolution. The instruments and their setup were identical to those employed and described in the preceding paper.<sup>6</sup>

*Time-resolved emission.* The excitation wavelength was set at 420 nm where only the anions absorb. Each sample was prepared in a 2-mm cuvette with a concentration of 50  $\mu$ M. For each anion, a single emission band was observed (e.g., see spectra of the anions of **5** and **9** in Figure 8). During the short time window of observations (Figures 8a,c), the emission quickly ( $< 10$  ps) reached the maximum intensity and stayed constant over the remainder of the observation. No shift of the TE band was observed for anion **5** in either time windows (Figures 8a,b), while a red shift of the emission of anion **9** was discernable but unremarkable (Figure 8d). For the anions of Group I compounds **1-6**, the maxima of the emission bands were found to overlap at  $\sim 510$  nm. For anions of **7-9** that contain e-withdrawing substituents, the emission band appeared in longer wavelength regions. The anion of **8** (Group I) peaked at 535 nm, while the maxima of the anions of **7** and **9** (Group II) were found at  $\sim 580$  nm. The values of the emission maxima measured in the TE experiments are similar to those recorded in the steady state measurements (Table 1).

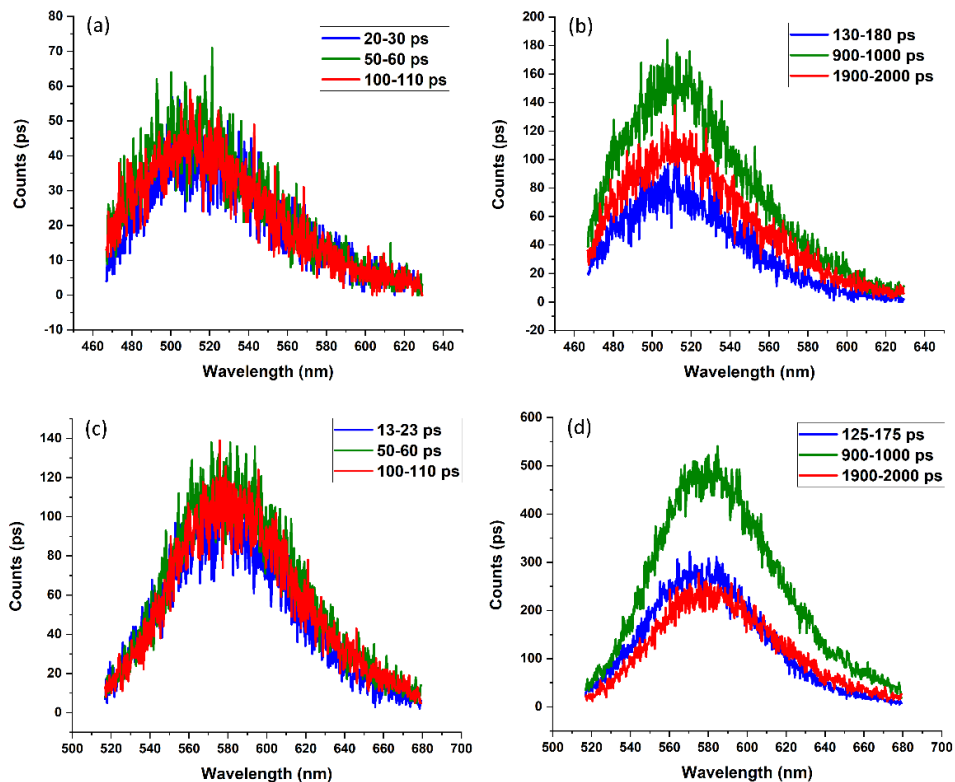


**Figure 8.** Emission spectra of the anions of **5** (R = H, a, b) and **9** (R = CN, c, d) taken at different time slices.  $\lambda_{\text{ex}}$  = 420 nm. [Dye] = 50  $\mu\text{M}$ ; DBU = 1 mM.

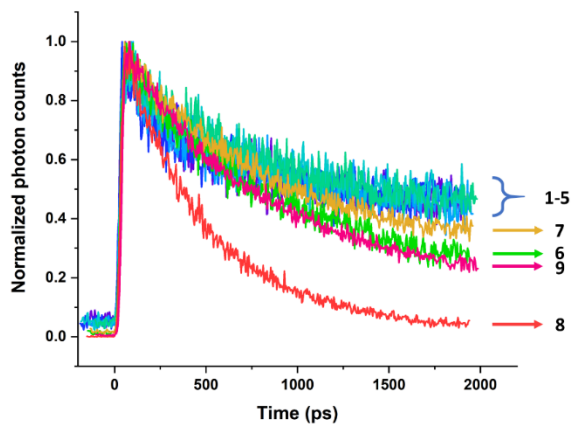


**Figure 9.** The normalized decays of anion emission bands of **1-9** in DMSO that were monitored using a streak camera at wavelength slices covering the maximum intensity.  $\lambda_{\text{ex}}$  = 420 nm; [dye] = 50  $\mu\text{M}$ ; [DBU] = 1 mM was used for deprotonation.

The collected time constants of the **PVHBO** anions are listed in Table S1. The values of the rise time  $t_1$  were extracted from the Track 1 data which has a temporal resolution of 2 ps. Based on the profiles of the time-dependent photon counts (Figure S4), there appear to be a slower, low-amplitude rise on the scale of tens of picoseconds. However, fitting for this component was not successful. The values of  $t_2$  and  $t_3$  were fitted from the Track 4 measurements that has a longer time window up to 2 ns. The rise of the emission ( $t_1$ ) mostly occurred within 5 ps, which is close to the instrument response. Consequently, it would have masked any processes that occur prior to this point. The time-dependent traces from Track 1 measurements are similar across all anions of the **PVHBOs** (Figure S4), suggesting that either similar photophysical events took place during the short time window, or the time resolution was not high enough to distinguish the initial fast events among the **PVHBOs**.

The  $t_2$  values of all compounds are in the range of hundreds of ps. The amplitudes of  $t_2$  of Group II anions (and that of anion of **8**) are larger than those of the Group I anions. For all anions there is an additional decay component ( $t_3$  in Table S1) that is longer than 2 ns (except anion **8** with a  $t_3$  of 0.9 ns), which is the duration of Track 4 measurements. For several anions,  $t_3$  values are too long to fit. Those include anions **1** ( $t_3 \sim 8$  ns), and **4, 5, 7**, of which the  $t_3$  values are marked as infinity ( $\infty$ ). The amplitudes of the  $t_3$  component of Group I anions remain unchanged as the monitoring emission wavelength increases, while those of Group II anions become slightly larger as the emission wavelength increases (See the decays of anions **5** and **9** at different wavelength slices in Figure S5, Table S2). The overall decays of the **PVHBO** anions observed at respective wavelengths of maximum intensity are shown in their normalized forms in Figure 9. The traces of the anions of **1-5**, all Group I members, closely resemble one another. In comparison, the Group II anions **7** and **9** show faster decays in the later stages. The anions of **6** and **8** appear to show behaviors that break the trend – the longest components ( $t_3$ ) of which are shorter than either of Groups I or II anions. The fluorescence lifetimes of selected anions (**1, 5, 7, and 9**) were also measured using the time-correlated single photon counting (TCSPC) technique. The single-exponential decay model was sufficient for fitting the decay curves, of which the Group I anions **1** and **5** had larger time constants than Group II anions **7** and **9** (Table S3). This observation is consistent with the overall slower decays of Group I anions (**1-5**) than the rest that were registered on the streak camera (see Figure 9). As an example of the insensitivity to oxygen, the decay trace of the anion of **1** (R = OMe) was not affected by degassing the sample via bubbling argon through for 2 minutes (Figure S6).

*Time-resolved absorption.* The anions of **PVHBOs** (50  $\mu$ M) were produced by the addition of 20 molar equivalents of DBU to the sample solutions in DMSO. The femtosecond time-resolved transient

absorption (fsTA) data were generated from exciting the samples at 420 nm where only the anions absorb. The experimental details of the fsTA experiments were described in the preceding paper.<sup>6</sup> Groups I and II anions show differences in both fsTA spectra and kinetics. Anions of **5** (R = H) and **7** (R = CO<sub>2</sub>Me) are used as examples of Groups I and II members, respectively, for describing these differences.

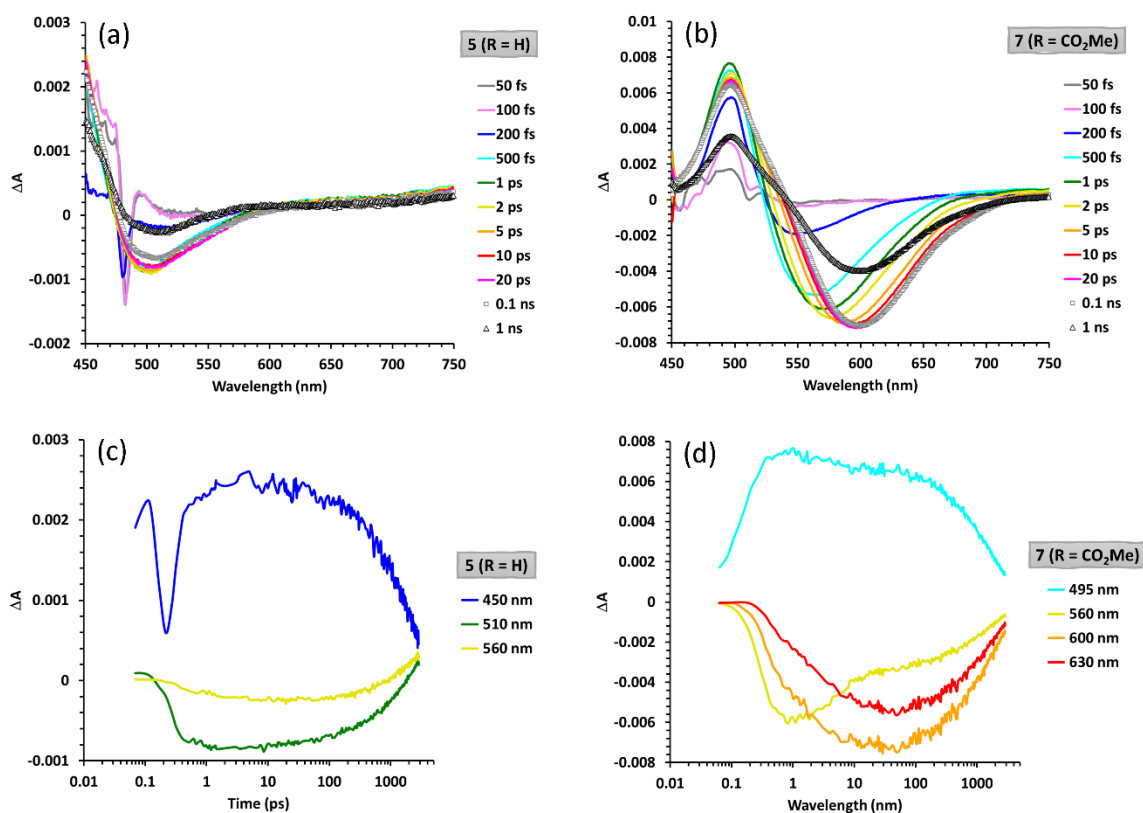


**Figure 10.** Femtosecond time-resolved transient absorption (fsTA) spectra (a, b) and decay traces (c, d) of the anions **5** (50  $\mu$ M, a and c), and **7** (50  $\mu$ M, b and d). [DBU] = 1 mM.  $\lambda_{\text{ex}}$  = 420 nm. Most of the TA spectra were selected from the early stage of the decays (50 fs – gray; 100 fs – violet; 200 fs – blue; 500 fs – cyan; 1 ps – green; 2 ps – yellow; 5 ps – orange; 10 ps – red; and 20 ps – magenta). The spectra taken at 0.1 ns (gray squares) and 1 ns (black triangles) are included as examples of those of later stages of the decays. The kinetic traces (450 nm – blue; 495 nm – cyan; 510 nm – green; 560 nm – yellow; 600 nm – orange; and 630 nm – red) followed the decays up to 2.8 ns. They are plotted on a logarithmic time scale so that the features from fs to ns are displayed.

In the first 200 fs of the fsTA experiment of anion **5** (gray, violet, and blue traces in Figure 10a), a sharp negative peak at  $\sim 470$  nm was observed, as well as a positive TA band on the higher energy side which was cut off at 450 nm. The negative spike at  $\sim 470$  nm is assigned as the stimulated Raman amplification from the solvent, based on its wavelength and ultrafast response similar to the instrument response (see the blue line, Figure 10c).<sup>14,15</sup> These features were replaced by a new TA band near 450 nm and a relatively broad negative band centering at 500 nm, the latter of which is the stimulated emission (SE) of the anion. These two main features are referred as blue and middle bands, respectively, according to the convention that was established in the preceding paper.<sup>6</sup> The 3D views of the fsTA data of anion **5** are shown in Figure S7a. The TA spectrum of anion **5** rapidly stabilizes after 500 fs, from which point on to 100 ps little change was detected (Figure 10a). No time-dependent shifts of any peak maxima (or minima) were observed.

The fsTA of anion **7**, which represents Group II compounds, afforded relatively strong and well-formed TA bands before the 200-fs mark (blue trace, Figure 10b). The positive blue band, which is an excited state absorption (ESA), at 500 nm decreased while the negative middle SE band starting at  $\sim 550$  nm shifted to eventually 600 nm over time. The wavelength maximum of the middle SE band red-shifted over a 10-ps span, in contrast to the blue ESA band of which no significant wavelength shift was observed. The kinetic traces plotted in Figure 10d contrast the decays of anion **5** (Figure 10c) in two aspects: 1) the stimulated Raman amplification band close to time zero that appeared in the decay traces of anion **5** was obscured in the traces of anion **7**, which has overall higher TA intensity than anion **5**; 2) the red shift of the middle SE band occurred in anion **7** but not that of **5**.

Both the blue ESA and the middle SE bands of the anions of Group II compounds are red-shifted from those of Group I anions (see the difference between Figures 10a,b). This level of difference between Groups I and II was not observed in the fsTA spectra of the neutral forms. Among all the features found in the fsTA spectra of neutral and anion forms, only the middle SE bands of Group II anions show a noticeable dynamic Stokes shift. This shift that occurs primarily over the first 10 ps was not captured in the TE experiments, which offer a lower time-resolution.

The kinetic traces of the blue ESA and middle SE bands (see Figure 10a,b) were fitted with multiexponential functions to yield the decay time constants (Tables S3-4). Three example fits of the blue ESA bands are shown in Figure S8. The ps and sub-ps time constants  $t_1$  and  $t_2$  of the blue bands of anions **1-6** (anions) were not fit with high confidence because the main feature in those decays during

the early stage is the stimulated Raman amplification (e.g., see that in the blue trace in Figure 10c), which cannot be fit by a multiexponential function, but has a temporal response comparable to the instrument response. The traces of anions **7-9** that contain e-withdrawing substituents produced two short time constants. The rise components ( $t_1$ ) that are 200 fs or shorter are close to the instrument response function (130 fs). Therefore, those are assigned to the direct excitations of the anions. The  $t_2$  values of **7** and **9** account for the dynamic Stokes shifts within the first  $\sim 10$  ps. A  $t_2$  of a similar magnitude was fitted from the decay of Group I anions, although without a dynamic Stokes shift. The longest time constants  $t_3$  of almost all anions are in the range of 1 to 2 ns. The value of  $t_3$  decreases as the anions transition to Group II. At the same time, the residual amplitude ( $y_0$ ) is disappearing, suggesting an overall faster restoration of Group II anions than Group I anions to the ground state.

The decays of the middle bands (Table S4) that are primarily accounted for by the SE can be divided into four segments: a sub-ps  $t_1$  within 0.1-0.2 ps for describing the rapid formation of the anion emitter, a single ps  $t_2$  component of vibrational relaxation, a tens of ps component to account for solvent-involved relaxation and perhaps a relatively short-lived excited state, and a ns component for emission. Note that the  $t_2$  components for **7-9** have amplitudes generally one order of magnitude larger than the other compounds, consistent with the appearance of dynamic Stokes shifts in the Group II compounds. A residual amplitude is needed for achieving a satisfactory fitting, suggesting the presence of either a long-lived excited state or the appearance of a new species resulted from photobleaching. If the values of two adjacent time constants are similar, or if the amplitude of one component is rather small, they could be merged with the adjacent component to still result in a satisfactory fit. For example, the  $t_2$  components of the anions **4** or **8** (0.6 and 0.7 ps, respectively, in Table S4) account for both the initial formation of the SE band and the vibrational relaxation process. The  $t_3$  values of the anions of **7-9** are found within 8-10 ps (Table S4), which coincide with the red shifts of the SE bands. The longest  $t_4$  component (in ns) of the middle SE band matches with the counterpart from the fitting of the blue ESA band, both of which are assigned to the radiative decay of the anion excited state.

**Computational studies.** The methods of computation were kept consistent with the ones described in the preceding paper.<sup>6</sup> The ground state of a **PVHBO** anion has two conformers in respect to the C-C bond between benzoxazole and phenoxide moieties. In one the phenoxide is “*cis*” to the azole nitrogen while in the other the phenoxide is “*trans*” to the same atom (Figure 11). These stereochemical definitions were consistent with those of neutral *cis*- or *trans*-enol forms of HBO.<sup>7</sup> Both conformers of the anion of **5** (R = H) were optimized at the DFT/B3LYP/def2-TZVPD level of theory using the COSMO

model to mimic a solvent environment of DMSO ( $\epsilon = 47$ ). The diffusion function was added in the basis sets to account for the charge in the structure. The *trans* isomer was slightly more stable (by 0.2 kcal/mol) than the *cis* isomer. The first two electronic transitions of the two conformers are similar in both excitation energy and oscillator strength (Table S5). For this reason, only the *trans* isomers of the **PVHBO** anions were computed, and the data from which are listed in this subsection.

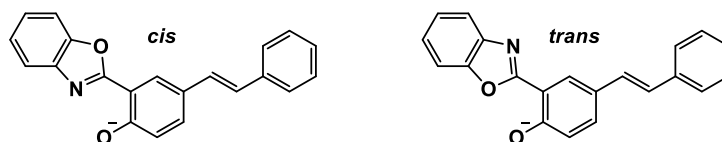


**Figure 11.** *Trans* and *cis* conformers of anion **5** (R = H). The *trans* conformer is 0.2 kcal/mol more stable in the ground state (DFT/B3LYP/def2-TZVPD), while it is 1.8 kcal/mol more stable than the *cis* conformer in the first excited state (TDDFT/B3LYP/def2-TZVPD).

**Table 2.** Two calculated lowest energy electronic transitions ( $\lambda_1$  and  $\lambda_2$  in nm), oscillator strengths (f), dominant MO contributions at the optimized ground state ( $S_0$ ) geometries (*trans* conformation) of the anions of **PVHBOs**, and the gaps between their  $S_1$  and  $S_2$  states ( $\Delta E$  in eV).<sup>a</sup>

| Comp. # | R                  | $\lambda_1$ (nm)/ $f_1$ | $S_1$ dom. Contr. <sup>b</sup> | $\lambda_2$ (nm)/ $f_2$ | $S_2$ dom. Contr. <sup>b</sup> | $\Delta E$ (eV) |
|---------|--------------------|-------------------------|--------------------------------|-------------------------|--------------------------------|-----------------|
| 1       | MeO                | 428/0.51                | H $\rightarrow$ L, 96%         | 394/0.95                | H $\rightarrow$ L+1, 95%       | 0.25            |
| 2       | Me                 | 424/0.62                | H $\rightarrow$ L, 98%         | 393/0.92                | H $\rightarrow$ L+1, 97%       | 0.23            |
| 3       | tBu                | 424/0.67                | H $\rightarrow$ L, 98%         | 396/0.89                | H $\rightarrow$ L+1, 97%       | 0.21            |
| 4       | F                  | 421/0.67                | H $\rightarrow$ L, 96%         | 395/0.71                | H $\rightarrow$ L+1, 95%       | 0.19            |
| 5       | H                  | 420/0.76                | H $\rightarrow$ L, 82%         | 396/0.72                | H $\rightarrow$ L1, 81%        | 0.18            |
| 6       | Cl                 | 425/1.04                | H $\rightarrow$ L, 63%         | 403/0.47                | H $\rightarrow$ L+1, 63%       | 0.16            |
| 7       | CO <sub>2</sub> Me | 475/1.32                | H $\rightarrow$ L, 96%         | 405/0.26                | H $\rightarrow$ L+1, 96%       | 0.45            |
| 8       | CF <sub>3</sub>    | 437/1.25                | H $\rightarrow$ L, 88%         | 403/0.26                | H $\rightarrow$ L+1, 87%       | 0.24            |

|           |     |          |            |          |              |      |
|-----------|-----|----------|------------|----------|--------------|------|
| <b>9</b>  | CN  | 473/1.35 | H → L, 96% | 403/0.26 | H → L+1, 96% | 0.46 |
| <b>10</b> | CHO | 519/1.25 | H → L, 98% | 403/0.28 | H → L+1, 97% | 0.69 |

a. (TD)DFT/B3LYP/def2-TZVPD level of theory. Solvation was considered using COSMO ( $\epsilon = 47$ , DMSO);  
 b. H – HOMO, L – LUMO; L1 – LUMO+1.

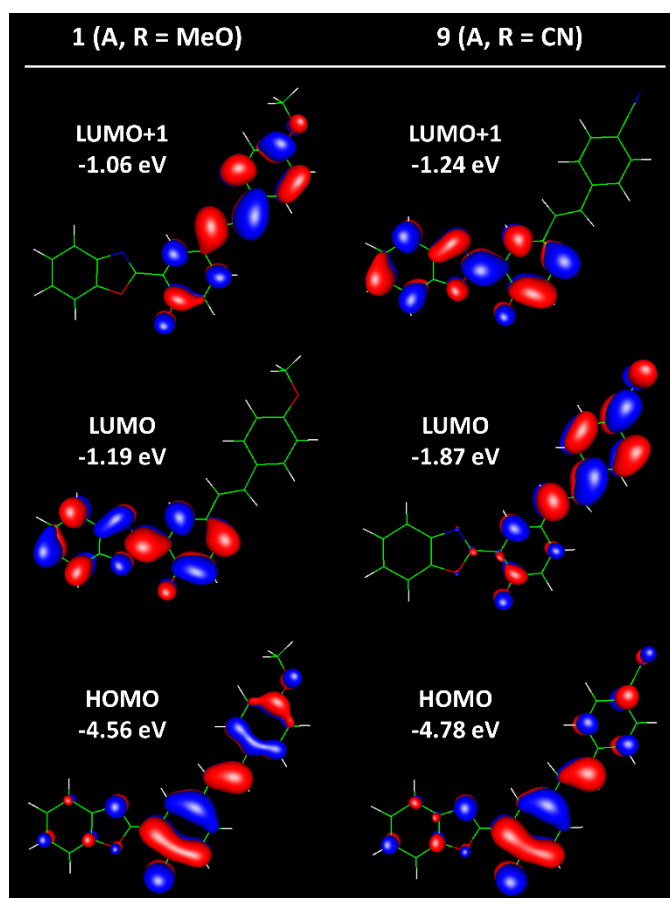


**Figure 12.** Frontier molecular orbital diagrams of the anion (A) forms of **1** (left) and **9** (right) calculated at the DFT/B3LYP/def2-TZVPD level of theory while solvation was considered using the COSMO model ( $\epsilon = 47$ , DMSO). The relative orbital energy values are listed.

The ground state ( $S_0$ ) geometries of anions **1-10** were optimized at DFT/B3LYP/def2-TZVPD level of theory, while the COSMO model was applied to account for solvation in DMSO. The excitation energy

values of the first two excited states ( $S_1$  and  $S_2$ ) and their respective oscillator strengths, calculated at the relaxed  $S_0$  geometries, are listed in Table 2. The major contributors to  $S_1$  and  $S_2$  are HOMO  $\rightarrow$  LUMO and HOMO  $\rightarrow$  LUMO+1 transitions, respectively, across the entire series of compounds. As the R group becomes more e-withdrawing, LUMO and LUMO+1 start to switch the molecular spaces that they occupy. As exemplified in Figure 12, the LUMO of anion **1** (R = MeO) was found on the HBO moiety while the LUMO+1 resides on the stilbenoid, while in anion **9** (R = CN), the LUMO and LUMO+1 almost entirely switched their places. Based on the substituent-dependent energetic order of LUMO and LUMO+1, the observed energies and the oscillator strengths of the absorption bands can be explained.

The calculated oscillator strength values are plotted in Figure 13a. The  $S_1$  oscillator strength (orange) increases as the R group becomes more e-withdrawing, while the  $S_2$  oscillator strength (blue) wanes. The former is an indicator of the transition probability of the HOMO  $\rightarrow$  LUMO transition, which increases as the LUMO shifts from the HBO moiety to the stilbenoid that overlaps better with the HOMO. At the same time, the HOMO  $\rightarrow$  LUMO+1 transition becomes less allowed as the LUMO+1 moves away from stilbenoid toward the HBO moiety, as the R substituent turns more e-withdrawing. The change of the relative oscillator strengths of  $S_1$  and  $S_2$  across the series leads to the switch of the stronger absorption from  $S_2$  to  $S_1$ . The calculated absorption energies also match well with the experimentally measured values ( $\lambda_{\text{max}}$  in eV in Figure 13b) and profiles of absorption bands. For anions **1-6**, the experimental  $\lambda_{\text{max}}$  values track closely with the calculated excitation energy to the  $S_2$  states, when the  $S_2$  states have relatively large oscillator strengths. For anions **7-10**, the calculated excitation energies of  $S_1$  states are more aligned with the experimental  $\lambda_{\text{max}}$  values, because the  $S_1$  transition has become more allowed than the  $S_2$  transition based on the calculated oscillator strengths.

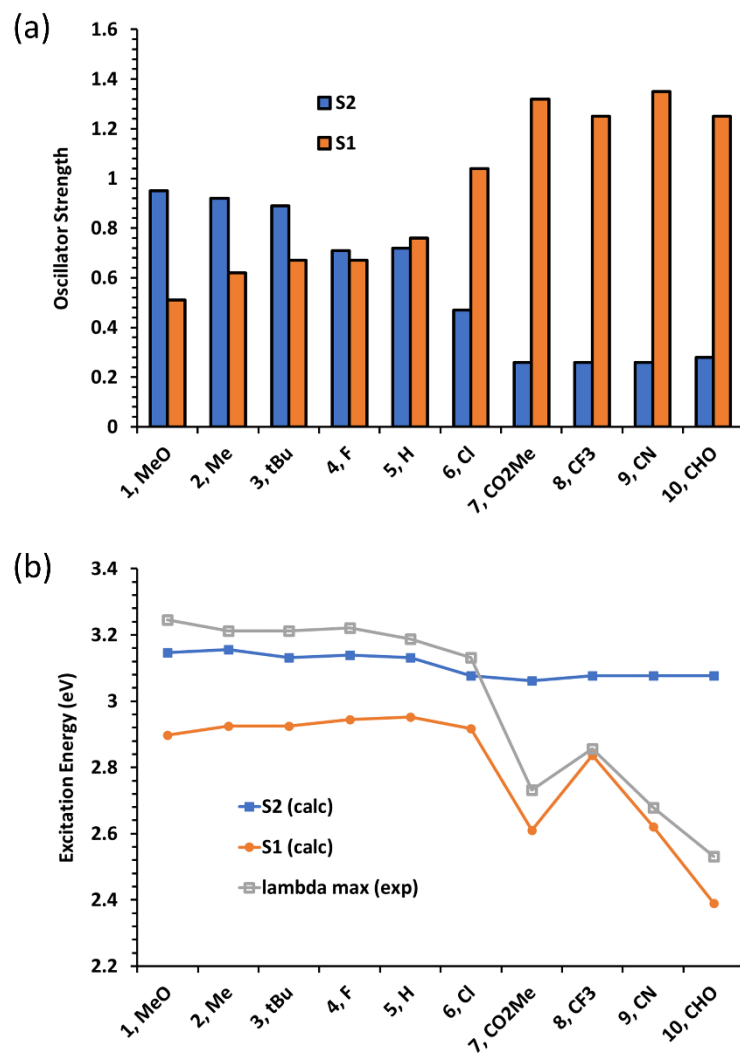


**Figure 13.** (a) Calculated oscillator strengths of the S<sub>1</sub> (orange) and S<sub>2</sub> (blue) states; (b) calculated excitation energies of S<sub>1</sub> (orange filled circles) and S<sub>2</sub> (blue filled squares) at the relaxed S<sub>0</sub> geometries, and the experimentally observed absorption maxima (gray open squares).

**Table 3.** Calculated lowest excitation energy ( $\lambda$  in nm), oscillator strength (f), and the dominant MO contribution at the optimized  $S_1$  excited state geometries (*cis* conformation).<sup>a</sup>

| Comp. # | R                  | $\lambda$ (nm) | f    | $S_1$ dom. Contr. <sup>b</sup> |
|---------|--------------------|----------------|------|--------------------------------|
| 1       | MeO                | 446            | 0.45 | H $\rightarrow$ L, 82%         |
| 2       | Me                 | 469            | 0.48 | H $\rightarrow$ L, 80%         |
| 3       | tBu                | 452            | 0.53 | H $\rightarrow$ L, 81%         |
| 4       | F                  | 440            | 0.46 | H $\rightarrow$ L, 84%         |
| 5       | H                  | 455            | 0.53 | H $\rightarrow$ L, 82%         |
| 6       | Cl                 | 438            | 0.50 | H $\rightarrow$ L, 84%         |
| 7       | CO <sub>2</sub> Me | 743            | 0.72 | H $\rightarrow$ L, 89%         |
| 8       | CF <sub>3</sub>    | 602            | 0.81 | H $\rightarrow$ L, 89%         |
| 9       | CN                 | 694            | 0.79 | H $\rightarrow$ L, 88%         |
| 10      | CHO                | 918            | 0.57 | H $\rightarrow$ L, 90%         |

a. TDDFT/B3LYP/def2-SVPD level of theory for optimization; PTED-COSMO-ADC(2)/def2-SVPD for single point excitation energy calculation at the optimized  $S_1$  geometry. Solvation was considered using COSMO ( $\epsilon = 47$ , DMSO); b. H – HOMO; L – LUMO.

The excited state ( $S_1$ ) geometries of the **PVHBO** anions were optimized at TDDFT/B3LYP/def2-SVPD level of theory in vacuum. Comparing to the ground state optimizations, a smaller basis set was selected for the purpose of saving computational cost. The single point excitation energies were calculated at the relaxed  $S_1$  geometries at ADC(2)/def2-SVPD level of theory, while solvation is considered with COSMO. The data are listed in Table 3. Larger deviations from the experimental emission maxima relative to the ground state calculations were expected considering the complications faced by excited state anion calculations.<sup>13</sup> The excitation energies of anions **1-6** were similar between one another and

overestimated from the experimental emission maxima, while those of anions **7-10** were progressively lower and were underestimated from the experimental values. The correlation between the R group and the excitation energy reproduces that of the experimental trend (Figure S9), in which the Group I anions emit within a narrow region of relatively short wavelengths, while the emission bands Group II anions are shifted progressively to the red as the R group becomes more e-withdrawing.

The HOMO  $\rightarrow$  LUMO transition is the major contributor to the  $S_0 \rightarrow S_1$  excitation at the relaxed  $S_1$  geometry (i.e., emission, Table 3). The HOMO and LUMO plots of the excited anions of **1** (**1a\***) and **9** (**9a\***), which represent Groups I and II anions, respectively, are shown in Figure 14a-b. The HOMO and LUMO of **1a\*** occupy the stilbenoid and HBO respectively, while those of **9a\*** take up almost the opposite physical residence. Neither the LUMO of **1a\*** nor the HOMO of **9a\*** involves much of the R substituent, while the LUMO of **9a\*** almost entirely localizes on the vinylbenzocnitrile moiety (Figure 14b). The HOMO of **1a\*** is more delocalized on the stilbenoid, within which the phenoxide is favored (Figure 14a). It is therefore reasonable to conclude that the emission of a Group II anion is more sensitive to the R substituent than a Group I anion based on the observation that out of the four FMOs shown in Figure 14, the R substituent is most involved in the LUMO of **9a\***.

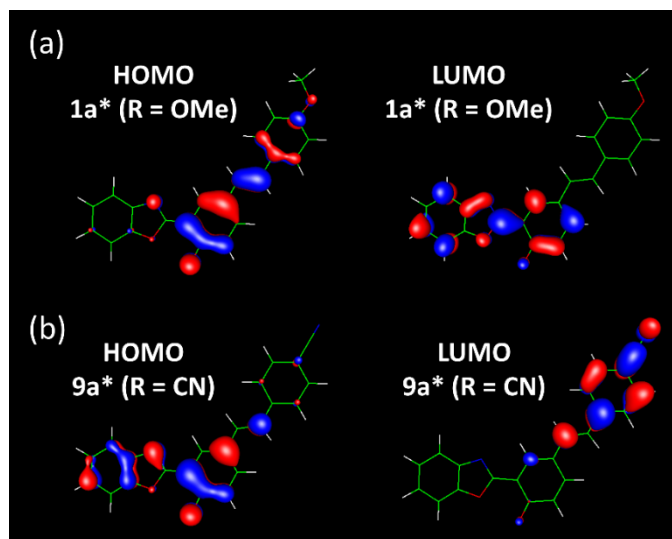


**Figure 14.** The HOMO and LUMO of anions of **1** (**1a\***, a) and **9** (**9a\***, b) at the relaxed excited state geometry calculated at the DFT/B3LYP/def2-SVPD level of theory while solvation was considered using the COSMO model ( $\epsilon = 47$ , DMSO).

## Discussion

**Anions of ESIPT fluorophores.** Although anions are major emitters of several classes of fluorophores,<sup>13</sup> the photophysical properties of anionic organic fluorophores have not been described as extensively as neutral compounds. Regarding ESIPT-capable fluorophores, one may find works on neutral species more readily than those on anions, which have occasionally been misidentified in the interpretations of anomalous emission band in the studies of neutral species. One of the earliest reports on the anion form of an ESIPT fluorophore is found in a series of publications on 3-hydroxyflavone (3HF, Figure 15) by Kasha and coworkers. 3HF is prone to solvent-assisted deprotonation (e.g., by water<sup>16</sup> or formamide<sup>17</sup>). The emission of the anion of 3HF was originally attributed to another form of the excited tautomer of the neutral 3HF.<sup>16,18</sup> Much effort, and years had gone by before the elusive proton transfer-driven photophysics of 3HF was clarified,<sup>16,17</sup> and from that one may appreciate that the spectroscopic studies of ESIPT compounds could be fraught with the interference by strongly interacting solvents and other impurities, and they require the utmost attention to details and rigorous control experiments to test all alternative possibilities to avoid misinterpretations.

Tinuvin P (Figure 15) is a highly photostable compound that is used as a UV light-absorbing additive to polymers. The photostability is attributed to the non-radiative decay of the excited state via ESIPT. The degradation of Tinuvin P over a long period of time, however, is postulated to originate from the photochemistry of the solvent adduct of the compound via an intermolecular hydrogen bond, which undergoes excited state deprotonation to afford an excited anion. Through this study, the absorption and emission of Tinuvin P anion were characterized.<sup>19</sup> Similar to Tinuvin P, aloesaponarin I (AS1 in Figure 15) is a UV-protective component of the aloe extract, which derives its photostability from its ESIPT capacity.<sup>20</sup> The anion of AS1 has an emission band with longer wavelengths than the emissions of both the normal and proton transferred tautomer.<sup>20</sup> The deprotonated AS1 was also found to be less photostable than its neutral form and therefore to engage in various photodegradation pathways.

Over the course of the studies on HBO by multiple groups, an anomalous long-wavelength absorption band had been noted and attributed to different species. It was later characterized as either the anion or a metal complex of the anion, which could be accidentally produced in strongly hydrogen bond basic solvents.<sup>8</sup> Similar anion chemistry was earlier characterized for 2-(2'-hydroxyphenyl)thiazole (HBT, Figure 15),<sup>21</sup> a compound that differs from HBO by a single atom. As the last example, phenyleneethynylene-substituted HBT (PEHBT, Figure 15) in polar solvents such as MeOH and DMF

exhibit a long absorption band which was characterized as that of the anion.<sup>22</sup> These are the several examples of anions of ESIPT fluorophores that are relevant to the current study.

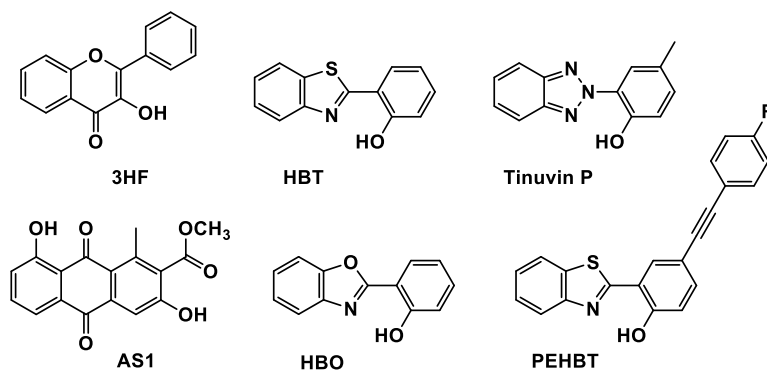


**Figure 15.** A few ESIPT fluorophores of which properties of anions were reported in literature.

**Absorption.** The absorption and emission properties of the anions of **1-10** can be explained based on the computed data. Each anion can be considered as a fusion of two chromophores – HBO and stilbenoid – both in deprotonated form. The absorption spectra of the anions shown in Figure 3 are dominated by the  $S_1$  and  $S_2$  states of each structure. These two states primarily consist (> 80% except anion **6**, see Table 2) of the transitions from the HOMO on the stilbenoid to the unoccupied molecular orbitals (LUMO or LUMO+1) on either HBO or stilbenoid (see examples in Figure 12). For most Group I anions (e.g., **1-5**), the  $S_2$  state (LUMO+1 on stilbenoid) is more allowed than the  $S_1$  state (LUMO on benzoxazole), while for Group II anions (e.g., **7** and **9**), the  $S_2$  becomes less allowed than the  $S_1$  (Figure 13a), because of the switch in energy of unoccupied molecular orbitals residing on benzoxazole (LUMOs in Group I) and stilbenoid (LUMOs in Group II) as the R group becomes more e-withdrawing.

The absorption spectral maxima of Group I anions **1-5** are insensitive to the R group, while those of a Group II anion drops quite readily as the R-substituent becomes more e-withdrawing. This difference in the level of absorption sensitivity to the R group may be rooted in the dependence, or otherwise, of frontier molecular orbitals on the R group (Figure 16a). The HOMO energies of all anions are confined in the narrow range of -4.8 to -4.5 eV (blue circles in Figure 16a). The energies of LUMO (-1.2 to -1.3 eV) and LUMO+1 (-1.1 to -1.2 eV) of Group I anions **1-6** are close to one another in addition to being

insensitive to the identity of R (right hemisphere of the radar plot in Figure 16a). The closeness between LUMO and LUMO+1 in anions **1-6** suggests that the  $S_1$  (principally HOMO  $\rightarrow$  LUMO transition) and  $S_2$  (principally HOMO  $\rightarrow$  LUMO+1 transition) states are coasting on the edge of a “phase transition”, and foretells a rather dramatic change of behavior as the R group becomes further e-withdrawing. The LUMO level of an anion carrying an e-withdrawing group (**7-10**) is noticeably lower than the former group (**1-6**), and decreases (except **8**) as the R group increases on the Hammett scale. The analysis of the correlations of FMO energies to the R group offers a good explanation to the key features of experimentally observed absorption spectra – namely, the absorption maxima of anions **1-5** coincide within a narrow range of the short wavelength region, while those of **6-10** are progressively longer as the R becomes more e-withdrawing (Figure 3).

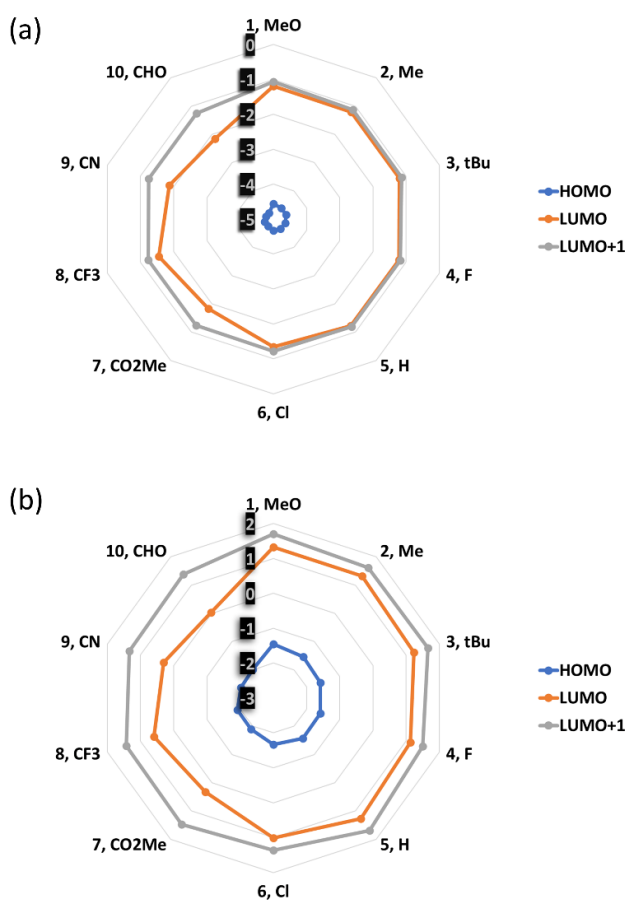


**Figure 16.** The calculated FMO energies in eV ((TD)DFT/B3LYP/def2-TZVPD) of anions **1-10** displayed in radar charts at  $S_0$  (a) and  $S_1$  (b) geometries. The scales in eV are shaded.

**Emission.** The FMO dependence on the R group calculated at the  $S_1$  geometries (Figure 16b) shows similarity to that at the  $S_0$  geometries (Figure 16a), which similarly explains the correlation between the emission maximum and the R group. The emission of Group I anions, i.e., the  $S_1$  excitation energy calculated at the relaxed  $S_1$  geometry, is dominated by the HOMO (alkoxide portion on stilbenoid) to LUMO (benzoxazole) transition (e.g., Figure 14a), which shows relative insensitivity to the R group (Figure 5). While for Group II anions, the LUMO is located primarily at the R-substituted phenyl end of the stilbenoid (e.g., Figure 14b), thus giving rise to the sensitivity of Group II anion emission to the R group. The localization of the fluorophoric component on a charge transfer type stilbenoid (“pushed” by the alkoxide and “pulled” by the e-withdrawing R group) could explain the dynamic Stokes shift of the SE captured in the fsTA data (e.g., Figure 10c), which is attributed to the solvent relaxation to accommodate the inversed dipole moment of the charge transfer-type stilbenoid upon excitation.

**Models that summarize the emission properties of PVHBOs.** The computational and time-resolved spectroscopic studies offer support to the following models that describe the emission properties of **PVHBOs**. When the R group is an e-donating group (EDG), the neutral fluorophore may exist with either an intramolecular hydrogen bond or an intermolecular hydrogen bond with a solvent molecule. Both forms could be excited with photons of similar energy, while the former would undergo ESIPT to afford the green keto emission whereas the latter is the source of the enol emission in the blue region, as described in the preceding paper.<sup>6</sup> Upon deprotonation, the anion absorption moves into the visible blue region, while it emits near 500 nm.<sup>13</sup> The fluorescence decays of the anions bear more similarities to that of the solvated enol than the keto form, suggesting a similarity in the electronic structure of the excited anion and the solvated enol. All three excited state species have similar FMO arrangements – HOMO resides on the stilbenoid while LUMO occupies the HBO component as shown by the colors in Figure 17. Of the EDG-substituted **PVHBOs**, the absorption and emission spectra coincide in their respective spectral regions (see the ranges included in Figure 17) regardless of the nature of the substituent.

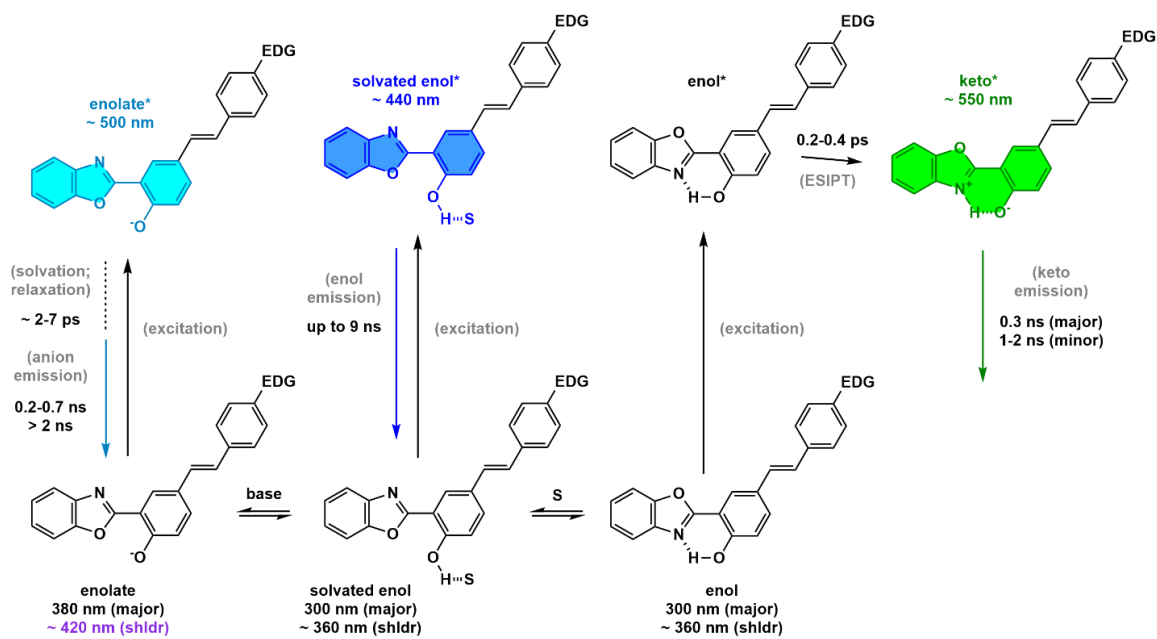


**Figure 17.** The structures that account for the emission properties of **PVHBOs** with an e-donating substituent (EDG). The LUMO component of an excited state is marked by the emission color of the respective species (The HOMO is invariably localized on the stilbenoid component at the  $S_0$  geometries). The absorption and emission maxima (or shoulder) are listed and marked with a matching color when falling within the visible spectrum. The excited state decays are also noted.

The model that describes the emission behaviors of **PVHBOs** with an e-withdrawing (EWG) substituent is shown in Figure 18. The space that the LUMO occupies in each excited species is marked by the color that matches the relevant emission. The observations of the neutral species were listed in the preceding paper and are not repeated here. With an EWG, the anion of a **PVHBO** behaves photophysically like a push-pull stilbenoid, on which both HOMO and LUMO orbitals are found (at the  $S_0$  geometry). The dynamic Stokes shift within 10 ps of excitation that is uniquely observed in the fsTA experiments is a consequence of the molecular dipole moment change of the charge transfer stilbenoid fluorophore upon excitation.

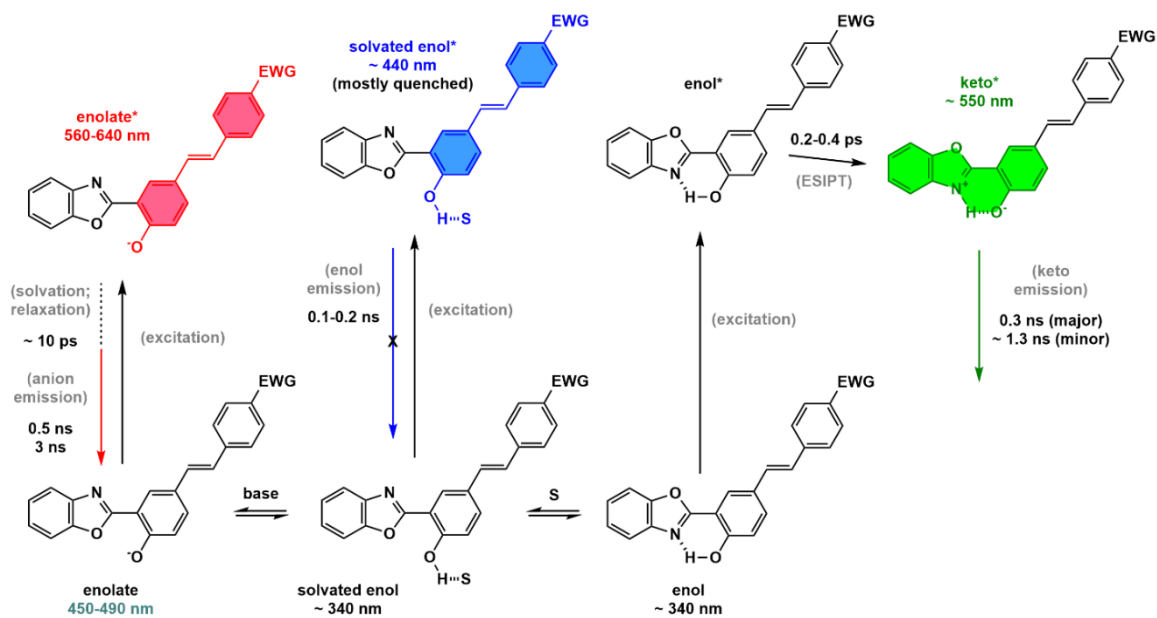


**Figure 18.** The structures that account for the emission properties of **PVHBOs** with an e-withdrawing substituent (EWG). The LUMO component of an excited state is marked by the emission color of the respective species (The HOMO is invariably localized on the stilbenoid component at the  $S_0$  geometries). The absorption and emission maxima are listed and marked with a matching color when falling within the visible spectrum. The excited state decays are also noted.

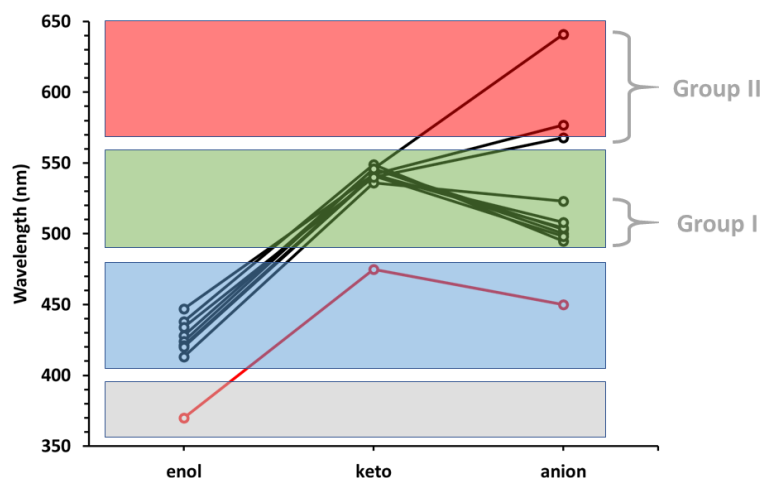


**Figure 19.** The sensitivities of enol, keto, and anion emission wavelengths of **PVHBOs** to the R substituent. As a reference, the respective values of unsubstituted HBO are 370, 475, and 450 nm as measured under identical conditions, which are shown as the red markers and line.

**Visible spectrum coverage by the emissions of PVHBOs.** The unsubstituted HBO is capable of emission from three different species – enol (E), anion (A), and keto (K). The E band centers at 370 nm in the UV region, while the A and K bands are found in blue to cyan region of the visible spectrum – 450 and 475 nm, respectively (red markers and line in Figure 19). When the 5'-position of HBO is substituted with an e-donating phenylenevinylene group to afford the Group I **PVHBOs**, all emission bands shift to longer wavelength regions while the order of E, A, and K remains unchanged (Figure 19). DMSO drives the emission to the enol (E) band, while in DCM only the keto (K) band is seen. When the 5'-position of HBO is substituted with an e-withdrawing phenylenevinylene group to afford Group II **PVHBOs**, two major spectral changes occur: (1) the A band moves to a wavelength that is longer than those of both E and K bands. (2) The K band appears to be more abundant, even dominating in a hydrogen bond-basic solvent such as DMSO. The latter is, as described in the preceding paper, attributed to the hydrogen bonding-mediated quenching of Group II enol emission, which amplifies the K band.

The sensitivity of the emission colors of **PVHBOs** to substituent is plotted in Figure 19. The emission wavelengths of enol and keto forms are the averages of the values acquired in various solvents, while the anion emission wavelengths were measured in DMSO using DBU (20 molar equivalents) as the base. For differently substituted **PVHBOs**, neither the enol nor keto form is sensitive to the substituent. The former clusters in the blue region of the visible spectrum while the latter peaks in the green section. On the contrary, the anion emission is sensitive to substituent – an e-withdrawing substituent, i.e., those carried by Group II **PVHBOs**, pushes the anion emission to a longer wavelength position than the neutral forms of both enol and keto emissions.

## Conclusion

This article, together with the preceding one, offer a comprehensive account on the optical properties of 5'-phenylenevinylene-substituted 2-(2'-hydroxyphenyl)benzoxazoles (**PVHBOs**). These compounds can be considered as a fusion of two fluorophores – the ESIPT-capable HBO and the stilbenoid on the 5'-axis of the compound. Three emission bands can be produced which are attributed individually to the enol, keto (the excited state tautomer), and the deprotonated anion species in the first singlet excited state. The emission wavelength maximum and relative abundance of each band depend on both the solvent and the R-substituent on the phenyl group. Depending on the nature of the R group, the studied compounds are separated into Groups I (R is e-donating) and II (R is e-withdrawing). The keto emission of all **PVHBOs** results predominately from the intramolecularly bonded species (solvent-mediated ESIPT in EtOH is likely), whereas their abundances are maximized in non-hydrogen bonding solvents. The major distinctions between Groups I and II compounds are revealed in the enol and anion emission properties in a hydrogen bonding solvent, such as DMSO. A Group I compound affords the enol emission as the major component in DMSO, while the enol emission of a Group II compound is quenched via the strong hydrogen bond with solvent in the excited state. The anion emission of a Group I compound exhibits insensitivity to the e-donating R substituent, while the energy of the emission of a Group II anion decreases as the R becomes increasingly e-withdrawing. Fluorescent dyes capable of multiple emission have been studied in the context of and employed in an increasing volume of applications from bioimaging to energy-efficient illuminations. In this work, the dependencies on R and solvent of the multiple emitting **PVHBOs** are explained by both ultrafast time-resolved spectroscopic observations and computational results, which yield predictive models that could correlate structure to emission color, relative abundance, and brightness of similar multiply emitting dyes.

## Author information

### Corresponding author

**Lei Zhu** – Department of Chemistry and Biochemistry, Florida State University, 95 Chieftan Way, Tallahassee, FL 32306-4390, USA; orcid.org/0000-0001-8962-3666; Email [lzhu@fsu.edu](mailto:lzhu@fsu.edu)

## Authors

Joseph J. M. Hurley

Quinton J. Meisner - Current address: Chemical Sciences and Engineering Division, Argonne National Laboratory, Lemont, Illinois 60439, United States of America

Peijun Guo

Richard D. Schaller – Center for Nanoscale Materials, Argonne National Laboratory, Lemont, IL 60126

David J. Gosztola – Center for Nanoscale Materials, Argonne National Laboratory, Lemont, IL 60126

Gary P. Wiederrecht – Center for Nanoscale Materials, Argonne National Laboratory, Lemont, IL 60126

## Notes

The authors declare no competing financial interest.

## Acknowledgements

This work was supported by the National Science Foundation (CHE1566011 and CHE1955262 to L.Z.). We thank the NSF-Research Experiences for Undergraduates (REU) Sites program. This material is based upon work supported by the NSF under Grant No. CHE-1659661. Use of the Center for Nanoscale Materials, an Office of Science user facility, was supported by the U.S. Department of Energy, Office of Science, Office of Basic Energy Sciences, under Contract No. DE-AC02-06CH11357.

**Supporting Information.** The Supporting Information is available free of charge at <https://pubs.acs.org/doi/XXXX>.

Syntheses and characterizations; additional steady state absorption and emission spectra; methods of ultrafast time-resolved emission and absorption spectroscopies; additional time-resolved absorption and emission spectra and kinetic decay traces; tables of lifetimes and amplitude values extracted from the time-resolved spectroscopic experiments; methods of computation; additional computed figures.

## References

- (1) Kasha, M. Proton-Transfer Spectroscopy. *J. Chem. Soc., Faraday Trans. 2* **1986**, *82*, 2379-2392.
- (2) Formosinho, S. J.; Arnaut, L. G. Excited-State Proton Transfer Reactions II. Intramolecular Reactions. *J. Photochem. Photobiol. A: Chem.* **1993**, *75*, 21-48.
- (3) Zhao, J.; Ji, S.; Chen, Y.; Guo, H.; Yang, P. Excited State Intramolecular Proton Transfer (ESIPT): from Principal Photophysics to the Development of New Chromophores and Applications in Fluorescent Molecular Probes and Luminescent Materials. *Phys. Chem. Chem. Phys.* **2012**, *14*, 8803-8817.
- (4) Demchenko, A. P.; Tang, K.-C.; Chou, P.-T. Excited-State Proton Coupled Charge Transfer Modulated by Molecular Structure and Media Polarization. *Chem. Soc. Rev.* **2013**, *42*, 1379-1408.
- (5) Zhou, P.; Han, K. Unraveling the Detailed Mechanism of Excited-State Proton Transfer. *Acc. Chem. Res.* **2018**, *51*, 1681-1690.
- (6) Meisner, Q. J.; Hurley, J. J. M.; Guo, P.; Blood, A.; Schaller, R. D.; Gosztola, D. J.; Wiederrecht, G. P.; Zhu, L. Triple Emission of 5'-(para-R-Phenylene)vinylene-2-(2'-Hydroxyphenyl)benzoxazole (PVHBO) – Part I – Dual Emission from the Neutral Species. **In Preparation.**
- (7) Abou-Zied, O. K.; Jimenez, R.; Thompson, E. H. Z.; Millar, D. P.; Romesberg, F. E. Solvent-Dependent Photoinduced Tautomerization of 2-(2'-Hydroxyphenyl)benzoxazole. *J. Phys. Chem. A* **2002**, *106*, 3665-3672.
- (8) Yuan, Z.; Tang, Q.; Sreenath, K.; Simmons, J. T.; Younes, A. H.; Jiang, D.-e.; Zhu, L. Absorption and Emission Sensitivity of 2-(2'-Hydroxyphenyl)benzoxazole to Solvents and Impurities. *Photochem. Photobiol.* **2015**, *91*, 586-598.
- (9) D'Andrade, B. W.; Forrest, S. R. White Organic Light-Emitting Devices for Solid-State Lighting. *Adv. Mater.* **2004**, *16*, 1585-1595.
- (10) Kamtekar, K. T.; Monkman, A. P.; Bryce, M. R. Recent Advances in White Organic Light-Emitting Materials and Devices (WOLEDs). *Adv. Mater.* **2010**, *22*, 572-582.
- (11) Bao, L.; Heagy, M. D. A Review of Single White-Light Emitters: The Quest for Picture Perfect Dyes in the Next Generation of Single Layer WOLED Displays. *Curr. Org. Chem.* **2014**, *18*, 740-772.
- (12) Meisner, Q. J.; Younes, A. H.; Yuan, Z.; Sreenath, K.; Hurley, J. J. M.; Zhu, L. Excitation-Dependent Multiple Fluorescence of a Substituted 2-(2'-Hydroxyphenyl)benzoxazole. *J. Phys. Chem. A* **2018**, *122*, 9209-9223.
- (13) Hurley, J. J. M.; Meisner, Q. J.; Huang, C.; Zhu, L. Hydroxyaromatic Fluorophores. *ACS Omega* **2021**, *6*, 3447-3462.
- (14) Devos, O.; Mouton, N.; Sliwa, M.; Ruckebusch, C. Baseline correction methods to deal with artifacts in femtosecond transient absorption spectroscopy. *Anal. Chim. Acta* **2011**, *705*, 64-71.
- (15) Ruckebusch, C.; Sliwa, M.; Pernot, P.; de Juan, A.; Tauler, R. Comprehensive data analysis of femtosecond transient absorption spectra: A review. *J. Photochem. Photobiol. C* **2012**, *13*, 1-27.
- (16) McMorro, D.; Kasha, M. Intramolecular Excited-State Proton Transfer in 3-Hydroxyflavone. Hydrogen-Bonding Solvent Perturbations. *J. Phys. Chem.* **1984**, *88*, 2235-2243.
- (17) Parthenopoulos, D. A.; Kasha, M. Ground State Anion Formation and Picosecond Excitation Dynamics of 3-Hydroxyflavone in Formamide. *Chem. Phys. Lett.* **1990**, *173*, 303-309.
- (18) Sengupta, P. K.; Kasha, M. Excited State Proton-Transfer Spectroscopy of 3-Hydroxyflavone and Quercetin. *Chem. Phys. Lett.* **1979**, *68*, 382-385.

- (19) McGarry, P. F.; Jockusch, S.; Fujiwara, Y.; Kaprinidis, N. A.; Turro, N. J. DMSO Solvent Induced Photochemistry in Highly Photostable Compounds. The Role of Intermolecular Hydrogen Bonding. *J. Phys. Chem. A* **1997**, *101*, 764-767.
- (20) Nagaoka, S.-i.; Uno, H.; Huppert, D. Ultrafast Excited-State Intramolecular Proton Transfer of Aloesaponarin I. *J. Phys. Chem. B* **2013**, *117*, 4347-4353.
- (21) Elsaesser, T.; Schmetzer, B. Excited-State Proton Transfer in 2-(2'-Hydroxyphenyl)benzothiazole: Formation of the Anion in Polar Solvents. *Chem. Phys. Lett.* **1987**, *140*, 293-299.
- (22) Xu, L.; Wang, Q.; Zhang, Y. Electronic effect on the photophysical properties of 2-(2-hydroxyphenyl)benzothiazole-based excited state intramolecular proton transfer fluorophores synthesized by Sonogashira-coupling reaction. *Dyes Pigm.* **2017**, *136*, 732-741.

## For Table of Contents Only

